

Tracking global large lake surface temperature variation from space using MODIS land surface temperature product

Boyu Zhao ^a, Zhongqiu Sun ^{a,*}, Min Wang ^b, Jia Du ^b, Kaishan Song ^{b,*}

^a School of Geographical Sciences, Northeast Normal University, Changchun 130024, China

^b Northeast Institute of Geography and Agroecology, Chinese Academy of Sciences, Changchun 130102, China



ARTICLE INFO

Keywords:

MODIS imagery
Bulk temperature
Global large lake
Water supply source

ABSTRACT

Water temperature monitoring plays a crucial role in the ecological functioning and biogeochemical cycling of aquatic ecosystems. Compared to conventional methods, satellite remote sensing provides a more efficient way to assess lake surface water temperature (LSWT) variations, particularly for large, remote water bodies. In this study, MODIS Land Surface Temperature (LST) product Level 3 (MOD11A2) is employed to analyze the spatiotemporal changes in LST for global inland water bodies with areas exceeding 25 km². This research aims to understand LSWT variations and identify the contributing factors. The findings indicate that during the nighttime, LSWT in different lakes ranges from -11 °C to 26 °C, while diurnal temperature differences (DTDs) range from 1.3 °C to 16.9 °C. Factors such as lake depth, surface area (or volume), altitude, geographical location, and water supply sources are shown to influence LSWT variations. This study addresses the gap in long-term LSWT research for lakes larger than 25 km² worldwide, providing valuable insights into the mechanisms driving LSWT changes in similar lake systems.

1. Introduction

The temperature of inland waters plays a crucial role in regulating various processes within aquatic ecosystems, including physical, chemical and biological processes (Verburg et al., 2003; Zhu et al., 2023). Lake temperature reflects its morphology, watershed and hydrological conditions and eventually influences the biology of aquatic organisms (Hulley et al., 2011; Noori et al., 2023). The thermal evolution and stratification patterns have a significant impact on the physical and chemical cycles of lakes. These patterns play a crucial role in governing the processes of lake production and decomposition (Zhang et al., 2014; Gibbons and Bridgeman, 2020). Lake surface water temperature (LSWT) is dynamic and changes seasonally and diurnally due to the annual insulation and air temperature variations. As climate change intensifies, lakes worldwide are experiencing unprecedented shifts in temperature patterns and trends (Woolway et al., 2020), with rising temperatures exerting a profound impact on lake ecosystems. Research indicates that climate-induced increases in surface water temperatures can enhance lake stratification, alter thermal cycling, and consequently affect water quality, biodiversity, and ecological functions (Adrian et al., 2009). The main factor influencing the variations in lake water

temperature is the absorption of solar energy and air temperature over the water surface. The absorption of light by water intensifies significantly as the light travels further through the water column, especially for wavelengths below 750 nm (Livingstone, 2003). High specific heat of water permits the dissipation of light energy and is accumulated as heat in the water column. However, the retention of heat is coupled with a number of factors that influence its distribution within a lake system, e.g., the wind speed, currents and other water movements, the morphology of the watershed, and gains and losses of water (Yin et al., 2023; Zhou et al., 2015).

Traditional lake temperature measurement techniques use in-situ data loggers, which provide precise, continuous information over time (Hulley et al., 2011). However, their applicability is limited to specific locations, making them incapable of capturing larger-scale temperature variations. In contrast, satellite thermal infrared (TIR) remote sensing has good capabilities to examine the LSWT changes in lakes and harsh environments at global scale (Hulley et al., 2011; Jungkeit-Milla et al., 2024; Schneider and Hook, 2010; Trumpickas et al., 2015; Wang et al., 2025). TIR remote sensing has been widely applied for mapping LSWT and circulation patterns in lakes with different satellite sensors (Schneider and Hook, 2010). Significant progress has been made in

* Corresponding authors.

E-mail addresses: sunzq465@nenu.edu.cn (Z. Sun), songkaishan@iga.ac.cn (K. Song).

recent years toward understanding global LSWT dynamics using remote sensing. While foundational studies like [Bussières et al. \(2002\)](#) and [Schneider and Hook \(2010\)](#) established early methodologies for LSWT retrieval, recent advances have enabled comprehensive analyses across larger spatial and temporal scales. Notably, [Tong et al. \(2023\)](#) demonstrated that global lakes are warming more slowly than surface air temperatures due to enhanced evaporation, highlighting the importance of hydrological-atmospheric feedbacks. [Korver et al. \(2024\)](#) compiled surface water temperature observations for 1.4 million lakes worldwide, revealing systematic warming trends across diverse lake types. While several studies have analyzed the spatiotemporal variation trends of LSWT in specific regions ([Huang et al., 2023](#); [Holley et al., 2011](#); [Trumpickas et al., 2015](#); [Yang et al., 2022](#)), limitations remain in understanding the underlying driving mechanisms ([Ptak et al., 2022](#)). For example, the combined effects of lake morphology, climate, and hydrology on LSWT trends, and long-term (multi-decadal) patterns for large lakes ([Piccolroaz et al., 2024](#)). This study utilizes satellite observation data to investigate the global spatiotemporal distribution patterns of LSWT, quantification of Diurnal temperature differences (DTDs) of LSWT and their spatial patterns, systematic evaluation of multiple controlling factors (depth, elevation, climate zone, etc.) for large lakes. These contributions provide a mechanistic framework for predicting LSWT responses to climate change and inform ecosystem management strategies.

In this article, a total of 12,978 composites of MODIS imagery data were processed and analyzed, covering the terrestrial area of the world. The characteristics of LSWT 2446 lakes with area greater than 25 km² were examined to determine its spatial feature associated with climate, landscape characteristics, and hydrologic conditions. This study aims to achieve the following objectives: (1) analyze the variations in lake LSWT globally using time series MODIS LST data from 2015; (2) compare the behavior of LSWT in 46 large lakes with different morphological conditions from 1 January 2001 to 31 December 2021; and (3) investigate the inter-annual temperature change rate of some typical lakes and examine the potential impact factors that regulate the LSWT spatial pattern and its temporal variations for these selected typical lakes. Most of the world's freshwater lakes lack long-term, continuous water temperature monitoring data, leading to considerable uncertainty in assessing the impact of LSWT changes on regional water resource management and ecosystem services ([Jeppesen et al., 2014](#); [Woolway et al., 2020](#)). Conducting global-scale LSWT research is not only crucial for advancing scientific understanding of how lake ecosystems respond to climate change but also essential for developing adaptive

management strategies and preserving ecosystem services ([Adrian et al., 2009](#); [Gizińska and Sojka, 2023](#); [Peng et al., 2022](#)). This study aims to provide a critical scientific foundation for global lake conservation and management by systematically analyzing the spatiotemporal variation patterns of LSWT and their ecological implications.

2. Materials and methods

2.1. Criteria of lakes concerned

Here, we conduct a global census of lake distribution and characterize lake thermal properties using images captured from space ([Pekel et al., 2016](#)). Considering the coarse grain size of MODIS LST product at nominal resolution of 1 km², lakes and some large reservoirs at global scale were extracted from Global Lakes and Reservoirs Database ([Lehner and Döll, 2004](#)). In total, 2446 lakes and reservoirs (referred to as lakes) with an area greater than 25 km² were chosen, and the distribution of water bodies is shown in [Fig. 1](#). As the most abundant lake distributed continent, 873 lakes are selected in North America, followed by Asia (861), Europe (273), South America (273), Africa (166), and Oceania (72). It is important to consider that certain lakes may not be chosen, even if they have an area larger than 25 km². This is because their elongated shoreline could lead to disconnection or land contamination when using the MODIS LST product at 1 km resolution over lake surface area ([Song et al., 2016](#)). The combined area of the 2446 lakes is approximately 1.53 million km², accounting for roughly 52 % of the global lake area ([Lehner and Döll, 2004](#)). To monitor the yearly pattern of LSWT for these 46 representative lakes chosen from various continents (refer to [Fig. 1](#)), the typical lakes in this study were selected based on the Köppen-Geiger climate classification and continental distribution characteristics to ensure typicality in climate and geographical distribution, including 10 lakes in Asia, 8 lakes in Europe, 8 lakes in Africa, 10 lakes in North America, 6 lakes in South America, and 4 lakes in Oceania; 16 lakes in low-latitude tropical regions, 25 lakes in mid-latitude temperate regions, and 5 lakes in high-latitude cold regions. Table S1 provides key parameters for 46 representative lakes.

2.2. MODIS LST product preprocessing

While the daily MODIS-Terra/Aqua LST (level 2, Collection 6) data set is more suitable for studying the thermal dynamics of lakes, there is a significant issue with cloud contamination that results in a high number of invalid pixels in the daily product ([Ke and Song, 2014](#); [Song et al., 2016](#)).

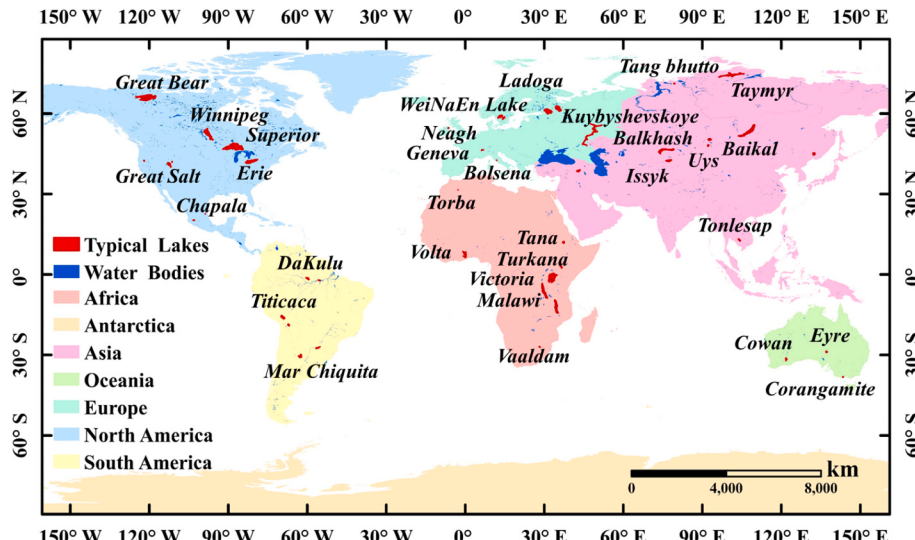


Fig. 1. The distribution of 2446 lakes across 6 continents (Antarctica is excluded).

2016). Thus, the MODIS LST 8-day composite product (level 3, MOD11A2) is preferred in this study, which is the integration of the average of daily LST observations in eight days with nominal resolution of 1 km². The data processing procedure is given in Fig. S1. Specifically, we used the MODIS Reprojection Tool (MRT) to perform mosaicking, resampling, and projection transformation, generating LST-Day, LST-Night, QC-Day, and QC-Night files. A 500-m buffer region of interest (ROI) was created based on lake vector files (for lakes with an area > 25 km²). We then clipped the QC files in ENVI and selected valid pixels according to the MODIS quality control standards (LST error ≤ 1 K, or LST error ≤ 2 K with emissivity error < 0.02). Finally, the corresponding LST data were extracted, and the DN values were converted into degrees Celsius using the following equation:

$$\text{New_DN} = \text{Old_DN}^* 0.02 - 273.15 \quad (1)$$

2.3. LST data analysis method

For validation purposes, this study utilized measured LSWT data collected from selected lakes across the Qinghai-Tibet Plateau during 2014–2015. Field measurements were obtained using a YSI EXO water quality multiparameter sonde, with temperature readings recorded at a depth of 0.3 m below the water surface. These measured data with daytime collected around 10:30 AM and nighttime around 10:30 PM local time. In this study, the threshold method was used to delineate water body boundaries, employing the spectral ratio of near-infrared (NIR) to green reflectance, which was derived from the MODIS reflectance product (MOD09Q1) at a nominal resolution of 500 m. This approach aimed to examine the relationship between water temperature and variations in water surface area by leveraging the distinct spectral characteristics of land and water in the NIR and green bands. To minimize contamination from the land-water interface and fluctuations in lake surface area, a 1-km offshore buffer zone was applied to exclude LST pixels along shoreline regions (Ke and Song, 2014). However, this buffering process occasionally resulted in disconnected zones in narrow lakes, which were subsequently corrected through manual inspection during data processing.

Cloud contamination introduces invalid pixels in the 8-day composite MODIS LST product (MOD11A2), necessitating appropriate methods for their removal (Wan et al., 2002). To address this issue, quality control images, labeled as QC-daytime and QC-nighttime, were also obtained, unreliable LST pixels over lakes were first filtered using QC information, followed by a median filtering approach applied to time-series LST data stacks to further smooth any remaining questionable pixels (Song et al., 2016). In the initial step, only pixels with an average LST error below 1 K (i.e., QC = 0, 1, 5, 17, and 21) were retained, while those with other QC values were discarded based on the LST data quality flag stored in the QC file. In the second step, a data cube was constructed by stacking 46 LST layers sequentially according to the Julian day. A median filtering algorithm was then applied to iteratively process each pixel, removing any remaining questionable values in the LST images (Fig. S2). In most cases, the 8-day composite contained more than 70 % valid pixels for daytime measurements, with only 138 out of 2890 images (5.5 %) having valid pixel coverage below 30 % (Fig. S3a). These low-coverage instances were primarily observed in Oceania during the winter season. Additionally, the nighttime MODIS LST product exhibited a higher number of valid images (Fig. S3b), consistent with findings from previous studies.

The median filter function is used to smooth LSWT, fill in blank values, and process extreme values. The formula of the median filter function is:

$$yk = \text{med}\{x(k-n), x(k-n+1), \dots, xk, \dots, x(k+n)\} \quad (2)$$

where med represents median, the median filtering method is to sort the pixels within the sliding filter window filter (2n + 1) by size, and the

output pixel value of the filtering result is defined as the median of the sequence.

Furthermore, the annual temperature change rates from MODIS LST data were analyzed by regressing them against the year of data acquisition using the following regression model (Zhang et al., 2014):

$$y = a + bx + e \quad (3)$$

where y represents the MODIS LST, x denotes the time series of years, e represents the residuals, a is the intercept, and b is the rate of temperature change, both of which are determined through least squares fitting.

2.4. Statistical analysis for LSWT

The annual averaged LSWTs for daytime and nighttime were derived by aggregating the 8-day LSWT composite for the corresponding time series and dividing by the number of time sequences. DTDs of LSWT were calculated by subtracting nighttime temperatures from daytime temperatures. The ice break-up starting point was determined by referencing the day-night averaged LSWT of lakes above 0 °C, while the freeze-up month ending point was determined by referencing the day-night averaged LSWT of lakes around 0 °C. In this investigation, the cumulative days were counted based on the median of the Julian day for each 8-day composite. The annual average LSWT maps were generated by averaging the 8-day maps on a pixel-by-pixel basis for each year.

2.5. Data collection

Latitude data was obtained from NASA's Earth Observing System Data and Information System (Justice et al., 1998), the study categorizes the world into six latitude zones for analysis. However, as no lakes were identified in the high latitudes of the Southern Hemisphere within the study area, no relevant results were obtained for this region. Climate zone data was sourced from the Köppen-Geiger Climate Classification (Peel et al., 1998), with the study area divided into five climate zones based on the Köppen classification. Elevation data was derived from the Advanced Spaceborne Thermal Emission and Reflection Radiometer Global Digital Elevation Model (ASTER GDEM) with a 30-m resolution (Ibrahim et al., 2020). The study classifies the world into five altitude zones. However, as no lakes in the study area were found above 5500 m above sea level, no relevant research results were obtained for this high-altitude region. The land-cover data were obtained from the Aerospace Information Research Institute, CAS. For analytical purposes, similar land use categories were merged, resulting in nine final classifications: grassland, farmland, forest, glacier and snow, shrubland, bare land, artificial land, wetland, and water. Since this study focuses on water, spatial analysis was conducted only on the eight land use types surrounding water.

3. Results

3.1. Validation of MODIS LST

In this study, measured LSWT data from selected lakes on the Qinghai-Tibet Plateau (2014–2015) were used for comparative validation with MODIS data. The geographic coordinates of the sampled lakes were spatially matched with MODIS imagery, and when a sampling point fell within a single MODIS pixel, the DN value of that pixel was extracted as the lake temperature representation. A total of 26 successfully matched lake samples underwent spatial analysis. A 3 × 3-pixel buffer was established, centering on the lake's central pixel, and the average value of all pixels within this window was computed as the final extracted temperature. The MODIS-derived temperature values were then compared with field observations to assess the accuracy of the remote sensing data. The results are shown in Fig. 2, with an R² of 0.87.

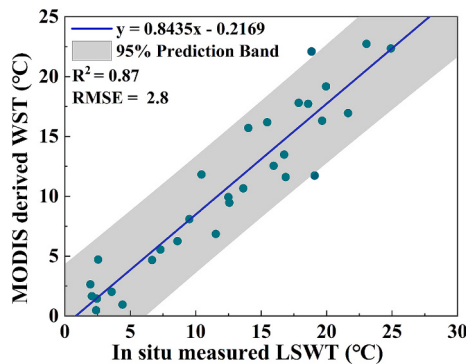


Fig. 2. MODIS LST product validation with both in situ measured data in 26 lakes across the Tibetan Plateau in 2014–2015.

A major source of error is the time mismatch between the measured data and the MODIS transit time, compounded by the fact that MODIS LST is an 8-day synthetic product. Potential sources of error include instrument noise, imbalance, sunlight, cloud pollution and surface reflectivity. In addition, the results in Fig. S4 show that the MODIS LST is moderately correlated with the LSWT from the GLAST dataset ($R^2 = 0.70$). To strengthen the validation, we further validated the MODIS LST using in situ LSWT data from hydrological monitoring stations in Chaohu Lake (Fig. S5), which demonstrated a high degree of accuracy ($R^2 = 0.92$). GLAST, as a globally integrated product, where it is significantly affected by atmospheric correction and spatial heterogeneity. In contrast, the validation over Chaohu Lake employed strictly spatiotemporal-matched in situ point measurements, effectively avoiding the mixed-pixel problem. These findings indicate that the MODIS LST product is suitable for analyzing global lake surface temperature trends.

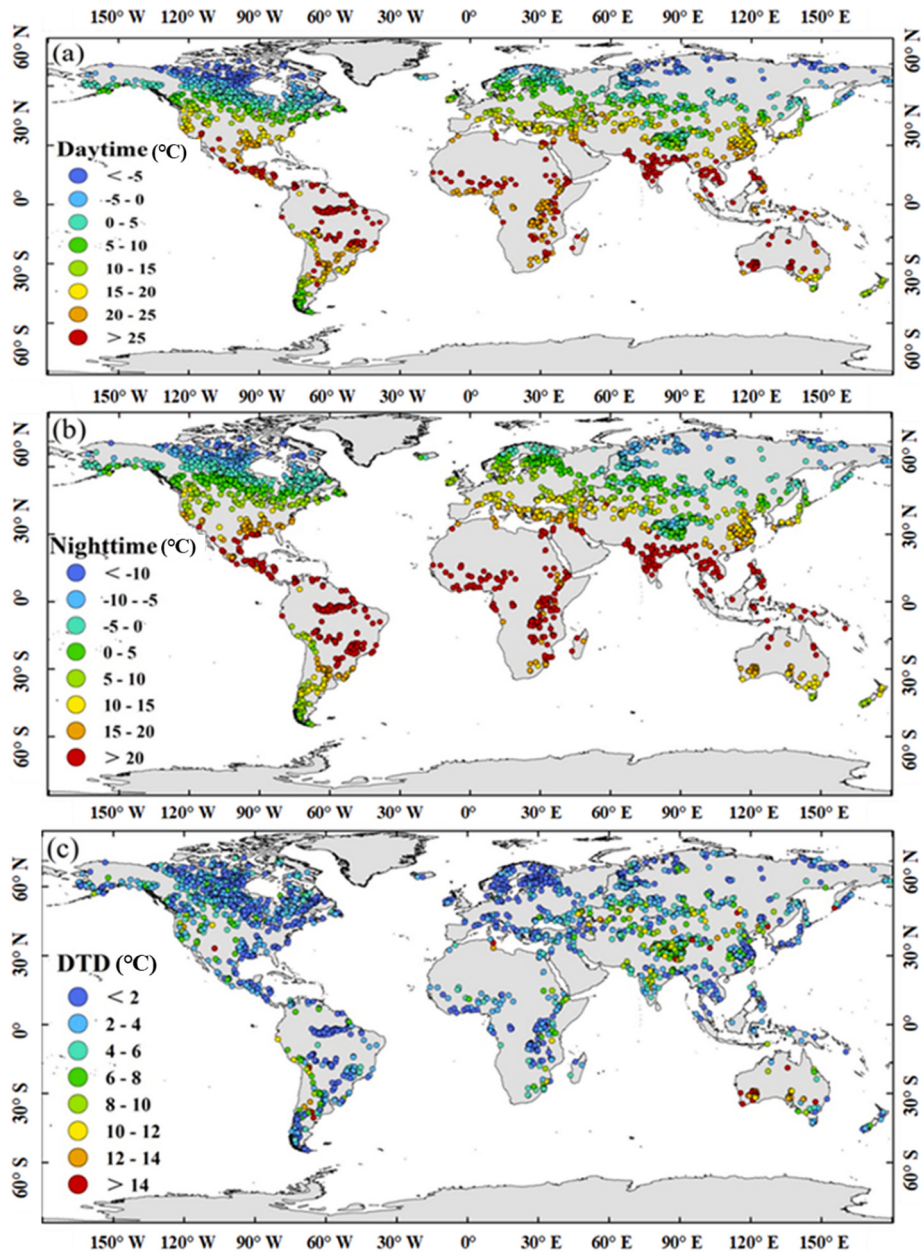


Fig. 3. The annual averaged LSWT pattern for lakes with area greater than 25 km², (a) daytime MODIS LST measurements, (b) nighttime MODIS LST measurements, and (c) the diurnal temperature differences (DTDs) at a global scale.

3.2. Global lake surface temperature pattern

Fig. 3a the annual average LSWT exhibits a clear contrast at the global scale for daytime MODIS LST measurements. Regions with high LSWT were found in various parts of the world, including the Iran Plateau, the South Asian Subcontinent, Indo-China Peninsula, South Asia, Australia excluding Hobart Island, most of Africa, Amazonia Basin in South America, and Central America. As expected, lakes at high latitude, especially those in the boreal or Taiga biomes, displayed low LSWT. Lakes on the Tibetan Plateau, known as the third pole of the world, also exhibit low LSWT. Lakes with LSWT ranging between 17 and 23 °C, 23–30 °C and greater than 30 °C were found intermixed around the Somalia Peninsula, West and South Australia, and the South Asian Subcontinent as well. This indicated that factors other than solar radiation and air temperature, such as water depth, volume, and water supply source may influence LSWT variations (Song et al., 2016). For nighttime MODIS LST measurements, a similar LSWT pattern is observed, as demonstrated in **Fig. 3b**. The temperatures range from −11 °C to 26 °C during nighttime. Notably, lakes in tropical climate zones tend to have higher temperatures (>22 °C) compared to those in temperate and cold climate regions at mid and high latitudes.

The DTDs of the 2446 lakes on a global scale are displayed in **Fig. 3c**. As anticipated, global lakes exhibited significant spatial variations in DTDs. Small DTDs were measured with water bodies located in cold climate regions at high latitude or tropical humid climate regions at low latitude. Examples include lakes in the northern territory of Canada, Scandinavian Peninsula, Amazonia, Congo Basin and the Great Rift Valley region of Africa, where either cold and humid or warm and humid climate prevail, resulting in smaller diurnal air temperature difference. Additionally, some small patches along the coastal regions also show low DTDs, indicating the prevalence of a marine climate. **Fig. 3c** shows that the distribution of large DTDs is primarily concentrated in arid or semi-arid regions. These regions include Central Asia, East Asia, Australia, the southern part of Africa, and the coastal arid region along the Andes of America, where significantly higher diurnal temperatures variations were experienced. Careful examinations also indicated that large and deep lakes, such as Lake Baikal, Lake Issyk-Kul, Lake Qinghai and Nam Co on the Tibetan Plateau, show less variability in DTDs. In contrast, lakes with large DTDs were generally found with small or shallow. When considering both daytime and nighttime LSWT patterns, it is reasonable to anticipate that lakes with significant water storage, such as Lake Baikal, Victoria, and Malawi, would exhibit less variability in terms of DTDs. To mitigate the impact of ice-covered lakes, the LSWT during the summer season (June to August) for daytime, nighttime, and DTDs were included in Fig. S6. In most cases, these patterns closely resemble the annual averaged values shown in **Fig. 3**, with the exception of the temperature range variation.

According to the data presented in **Table 1**, it is evident that the density of lakes in the mid latitude region of the northern hemisphere surpasses that of other regions. A significant majority, 69.7 %, of the selected lakes, amounting to 2446 lakes, are located in this particular

region. Furthermore, the collective area of these lakes measures 1,113,900.3 km², accounting for 72.2 % of the total lake area under investigation. The second region of high lake density (for lakes with an area > 25 km²) is situated in the low latitude of Southern Hemisphere, where 249 lakes are distributed, with a total lake area amounting to 198,918.5 km². According to daytime MODIS LST measurements, the minimum LSWT in the Northern Hemisphere is higher than that in the Southern Hemispheres. Likewise, the maximum temperature also exhibits the same trend, while the mean temperatures in both low latitudes of Northern and Southern Hemispheres are very close. For nighttime MODIS LST measurements, the minimum LSWT in the Southern Hemisphere is much lower than that in the Northern Hemisphere. Slightly higher temperatures for both the maximum and mean values are observed in both hemispheres. As anticipated, there is a significant variation in LSWT in the low latitude region of the Southern Hemisphere.

In the mid-latitude regions of both the Southern and Northern Hemispheres, there is a noticeable difference in temperature patterns. The Northern Hemisphere experiences significantly lower minimum and mean temperatures, while the maximum temperature remains relatively similar. Compared to the daytime MODIS LST measurements, similar trends are observed, though the difference are much smaller in the nighttime measurement. The Northern Hemisphere exhibits large variation (S-D = 8.07) compared to the Southern Hemisphere (S-D = 5.34). Only lakes in the high latitude of the Northern Hemisphere were examined in this analysis, as lakes from Antarctic were not included. Altogether, the temperatures of 155 lakes, with a total area of 47,257 km² were analyzed, and the only zone with mean LSWT below 0 °C is encountered in daytime MODIS LST measurement, while even lower LSWTs are recorded with nighttime MODIS LST measurements. Nevertheless, there are slight and nearly identical variations in LSWT observed in both daytime (S-D = 3.25) and nighttime (S-D = 3.31) measurements.

Fig. 4a displays the observed variations in daytime LSWT for lakes across different continents. North America and Asia have more lakes selected for characterizing LSWT due to their higher limnetic ratio. As two vast continents spanning a wide range of latitudes, larger LSWT ranges are observed for both Asia and North America. It also can be noted that lakes with lower temperature ranges (−10–0 °C and 0–10 °C) were more populous in these two continents. Comparing the numbers of lakes across Europe, Africa, and South America, it is interesting to note that each continent exhibits different ranges of LSWT. Europe, for example, has a greater abundance of water bodies with lower temperatures. On the other hand, Africa and Oceania are characterized by a prevalence of lakes with relatively higher temperatures. Careful examinations also indicated that large and shallow lakes, particularly ephemeral ones (Eyre, Corangamite, and Pan Lake), generally show extremely higher temperature. As shown in **Fig. 4b**, the nighttime shows a similar LSWT distribution to that measured in the daytime. However, lakes with higher daytime temperatures (> 30 °C) disappeared in the nighttime MODIS LST measurements.

Table 1
Statistics of LSWT for tropical, temperate and cold climatic zones in both Northern and Southern hemispheres.

Latitude range	North Hemisphere			South Hemisphere	
	67–90°	23–67°	0–23°	0–23°	23–67°
Lake Numbers	155	1644	193	249	205
Area(km ²)	47,257.30	1,113,900.34	123,968.72	198,918.50	40,272.15
Day					
Min	−11.65	−11.28	17.62	13.83	3.00
Max	1.46	39.63	42.66	40.60	39.37
Mean	−5.44	7.44	26.52	26.60	20.86
Std	3.25	9.08	3.05	4.87	8.64
Night					
Min	−12.93	−15.23	10.70	−2.03	−7.30
Max	0.77	25.05	28.58	26.66	24.07
Mean	−7.44	3.29	23.07	22.08	13.69
Std	3.31	8.07	2.23	4.50	5.34

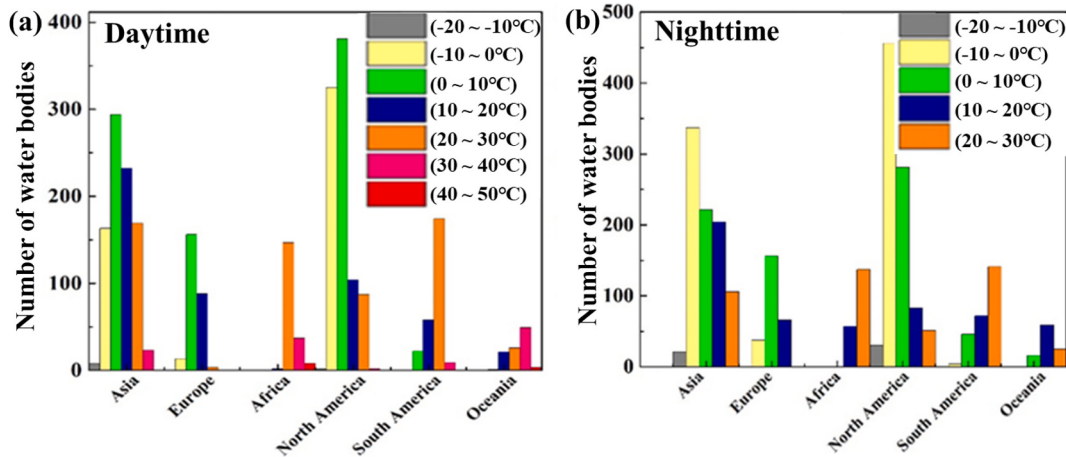


Fig. 4. Lake temperature distribution for different continents, (a) daytime MODIS measurement, and (b) nighttime MODIS measurements.

3.3. Inter-annual LSWT variations

The determination of global warming hot spot areas was based on the IPCC AR.5 report (2014), which considered the distribution of global lakes (Fig. 1). Typical lakes from each continent in these hotspot areas were selected to explore the inter-annual variations using the MODIS LST measurements from 2001 to 2021.

3.3.1. Typical lake from Asia

Fig. 5 illustrates the year-to-year fluctuations of LSWT for representative lakes in Asia from 2001 to 2021. Over the past 21 years, there has been a correlation between the annual daytime and nighttime LSWTs. Different lakes across Asia have shown varying trends. As the world deepest lake, Baikal shows a slight temperature increase, but it is not significant for daytime measurements (Fig. 5a), consistent with the findings by Hampton et al. (2008). As shown in Fig. 5b, a slight but insignificant increase trend is exhibited for the Lake Khar Us, located in

the Mongolia Plateau (see Fig. 1 for location). Similarly, the Lake Uvs, also in the Mongolia Plateau (Fig. 5e), shows a slight, though not significant, temperature increase trend during both daytime and nighttime. Over the past 21 years, Lake Balkhash (Fig. 5c) has displayed clear annual temperature fluctuations. There is a slight upward trend in both daytime and nighttime temperatures, although it is not considered significant. Located relatively close to Lake Balkhash, the alpine lake of Lake Issyk-Kul located in the Pamir Plateau shows an inverse annual variation, Lake Tonlesap, and very weak temperature decrease trend (Fig. 5d). Some lakes that experienced a notable increase in LSWT include Lake Khanka, Lake Van, Lake Taymyr, and Yang-Bhutto (refer to Fig. 1 for their locations). Both the daytime and nighttime measurements yielded similar results, with statistical significance ($p < 0.05$) (see Fig. 5f-i). Lake Tonlesap (5j) exhibits a subtle decline in temperature during both the day and night, although the change is not statistically significant.

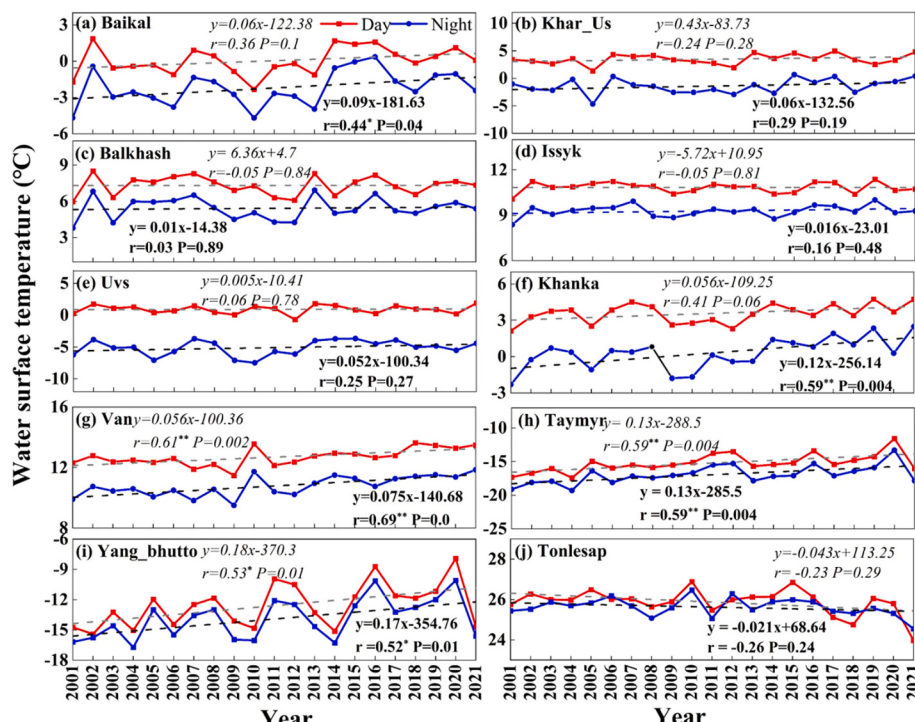


Fig. 5. Inter-annual temperature variations of lakes from Asia.

3.3.2. Typical lake from Europe

Fig. 6 illustrates the annual fluctuations of several representative lakes throughout Europe from 2001 to 2021. Fig. 6a-d clearly show the co-variation of annual daytime and nighttime temperatures for the four great lakes in northern Europe over the past 21 years. There is a noticeable upward trend in temperature. Significant temperature increases only observed for nighttime ($p < 0.05$) MODIS LST measurements for Lake Ladoga and Lake Vattern (Fig. 6a, c). Lake Ladoga, the largest lake in Europe, showed a slight increase but insignificant increase for the daytime measurement ($p > 0.01$). There was a slight increase in temperature observed for both Lake Onega and Lake Vanern, as well as for Lake Geneva and Lake Neagh, based on the MODIS LST measurements taken during both daytime and nighttime (Fig. 6b, d, e-f). However, these increases were found to be insignificant ($p > 0.05$).

3.3.3. Typical lake from Africa

Fig. 7a-d illustrates the annual fluctuations of the four largest lakes in the Great Rift Valley region of Africa. It is worth noting that there have been noticeable decreases in temperature trends based on the annual daytime and nighttime MODIS LST measurements over the past 21 years. For the greatest lake in Africa, the daytime and nighttime LSWTs over Lake Victoria shows the same trends (Fig. 7c), but the temperature decrease trend in nighttime ($p < 0.01$) is stronger than that in daytime ($p < 0.01$) measurements. Lake Tanganyika, being the second largest lake in Africa and the longest in the world, exhibits a remarkable similarity between its daytime and nighttime temperatures, as shown in Fig. 7b. A very significant temperature decrease trends are observed for both daytime ($y = -0.05x + 125.24$, $r = -0.83$) and nighttime ($y = -0.04x + 100.65$, $r = -0.8$) MODIS LST measurements. As shown in Fig. 7d, fluctuated but significant decreasing trends were observed for Lake Malawi in both daytime ($y = -0.025x + 74.09$, $r = -0.52$) and nighttime ($y = -0.02x + 75.69$, $r = -0.39$) of the MODIS LST measurements. Lake Turkana (Fig. 7a), the largest permanent desert lake and the world's largest alkaline inland water, experiences a noticeable decrease in temperature during the day according to MODIS measurements ($p < 0.01$). However, there is only a slight and insignificant decrease in temperature during the night based on MODIS measurements ($p > 0.01$). The Volta Reservoir in Ghana is the largest manmade water body in the world (8515 km^2). Similar trend with Lake Turkana is observed the reservoir, i.e., significant temperature decrease ($p < 0.01$)

was traced with daytime measurements, however, the decrease trend is not significant with respect to nighttime measurement (Fig. 7e). Fig. 7f and h illustrate that Lake Tana and Vaaldam exhibit minor decreases in LSWT when comparing daytime MODIS LST measurements. However, these decreases are not statistically significant ($p > 0.05$). On the other hand, no clear patterns can be observed with the nighttime measurements. The LSWT of Lake Torba shows a significant downward trend in daytime and nighttime (Fig. 7g, $p > 0.05$). Interestingly, the DTDs for the three lakes (Fig. 7f-h) exhibit similar pattern, i.e., larger DTDs (about $3\text{--}5^\circ\text{C}$) is observed, which is obviously different from the pattern presented in Lake Victoria, Tanganyika, and Lake Malawi, where close DTDs were exhibited.

3.3.4. Typical lake from North America

The four lakes shown in Fig. 8a-d are situated in the Nevada Mountain region, which experiences a predominantly arid climate. Similar annual LSWT variation trends are demonstrated for these four lakes, and slightly temperature increases were experienced for each lake. Great Salt Lake (Fig. 8a), known for its high salt content, shows an increase in LSWT based on both daytime and nighttime MODIS measurements. The increase is more pronounced during the daytime ($p < 0.01$) compared to the nighttime ($p > 0.05$). Lake Utah and Buir, Lake Upper Klamath (Fig. 8b-d) shows a slight temperature increase trend though not significant in daytime, but a significant increase trend exhibited in nighttime ($p < 0.05$). As the great lake situates the transient zone of the northern polar region, Lake Great Bear experiences slightly temperature increase with nighttime MODIS LST measurement, but not significantly; even weak trend is observed with daytime MODIS LST measurement. According to Fig. 8e, the LSWT for Lake Great Bear is consistently below freezing, suggesting that the lake is frozen for the majority of the year. It can be noted that the LSWT of Lake Winnipeg resembles that from Lake Great Bear, indicating the major regulating factor for both LSWT is similar. Fig. 8f-g illustrates significant annual fluctuations in LSWT both the great lakes Superior and Lake Winnipeg. Additionally, a noticeable decrease in temperature is observed for both lakes, although it is not statistically significant. Lake Erie, both daytime and nighttime measurements demonstrated temperature increase in the past 21 years. Situated in Mexico arid region, Lake Check para showed significant LSWT variation during the past 21 years, but inverse trend was exhibited with nighttime measurement showing temperature

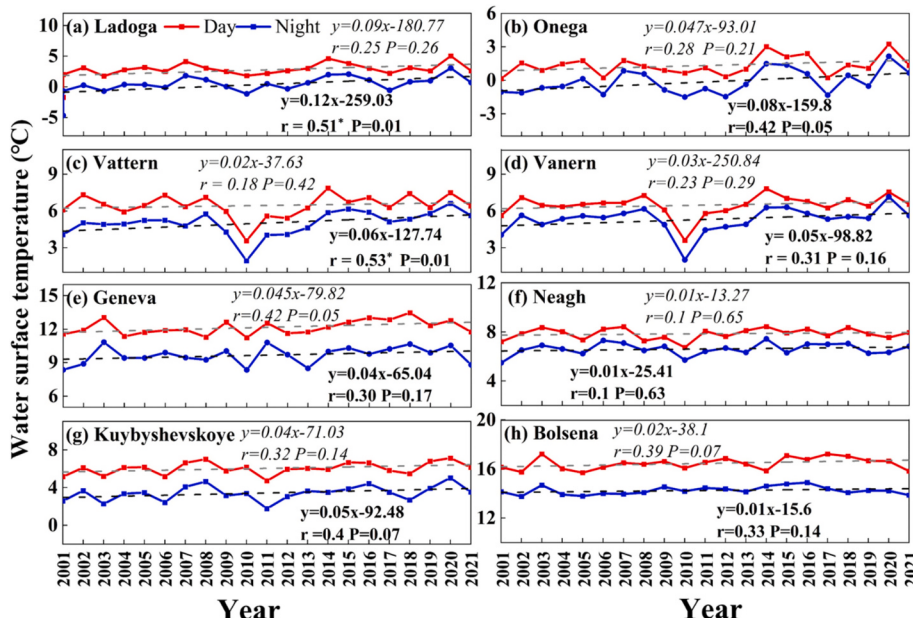


Fig. 6. Inter-annual temperature variations of lakes from Europe.

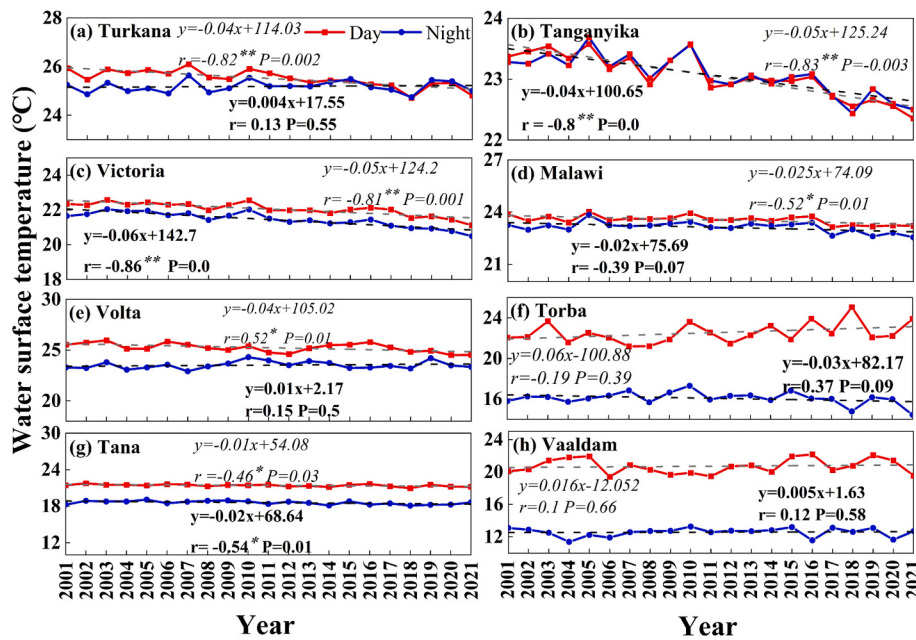


Fig. 7. Inter-annual temperature variations of lakes from Africa.

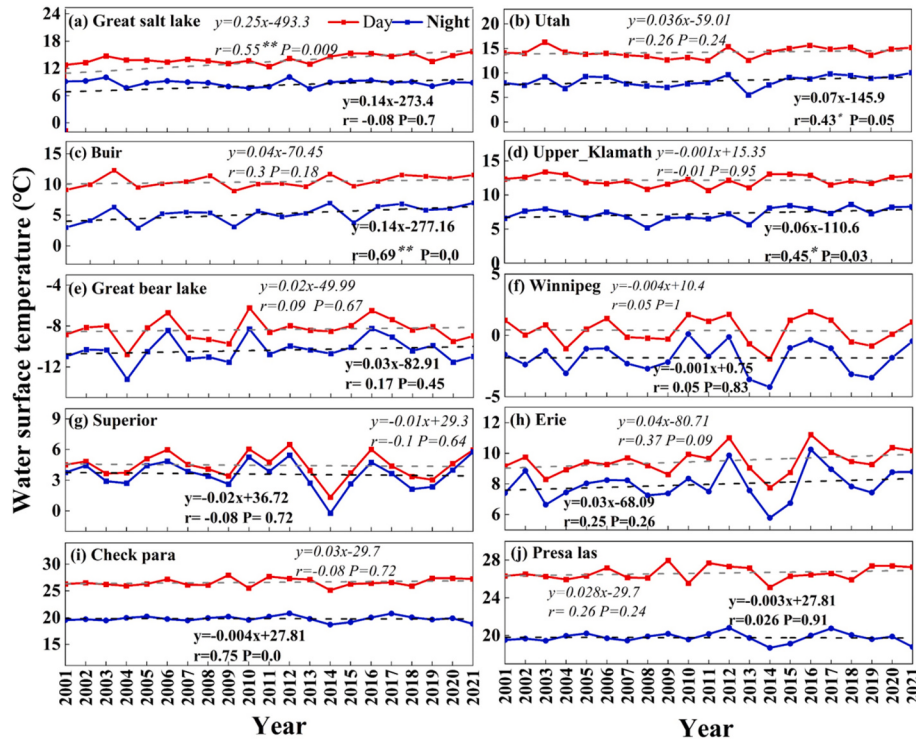


Fig. 8. Inter-annual temperature variations of lakes from North America.

decrease and daytime measurement showing temperature increase (Fig. 8i). Lake Presa Las is situated in close proximity to Lake Check para, resulting in a comparable annual variation pattern of LSWT, as shown in Fig. 8j. In this study, large lakes such as Lake Superior exhibited slower temperature changes, a phenomenon attributed to their vast water volumes and depths, which facilitate heat distribution and buffer the direct impact of external climate change on LSWT (Kraemer et al., 2021). In contrast, shallow lakes, due to their smaller volumes and shallower depths, generally warm more rapidly. This difference is closely linked to the heat capacity and thermal inertia of lakes,

with shallow lakes demonstrating greater sensitivity to climate change (Woolway and Merchant, 2019).

3.3.5. Typical lake from South America

When it comes to its size, Lake Titicaca ranks second only to Lake Maracaibo. However, in terms of volume, it takes the crown as the largest lake in South America. Not only that, but it also holds the title of being the highest navigable lake on the continent, with a surface elevation of 3812 m. As shown in Fig. 9a, an obvious temperature increase is observed with daytime MODIS measurement ($p < 0.05$),

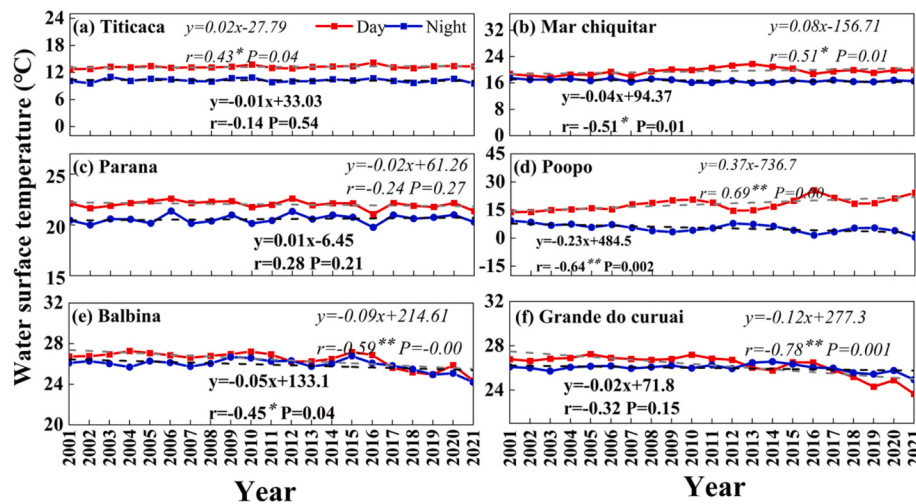


Fig. 9. Inter-annual temperature variations of lakes from South America.

while a slight but not significant increase temperature is revealed with nighttime measurement. Lake Mar Chiquitar (Fig. 9b) experienced marked surface area shrinkage ($-67 \text{ km}^2/\text{yr}$) in the past 40 years due to agricultural irrigation diversion the major inflow rivers, shows a slight temperature significant increase trend in daytime and nighttime ($p < 0.05$). There are no clear trends in the MODIS measurements for Lake Parana, both during the day and at night (see Fig. 9c). As for Lake Poopo (Fig. 9d), a large saline lake located in the shallow depression in the Altiplano Mountains at an altitude of approximately 3700 m. Interestingly, an inverse trend is observed for the temperature trend over Lake Poopo, e.g., a significant temperature increase trend is traced with daytime ($y = 0.37 \times -736.7$, $r = 0.69$, $p < 0.01$) MODIS measurement, while an inverse trend is exhibited with nighttime ($y = -0.23 \times +484.5$, $r = -0.64$, $p < 0.01$) measurement. Fig. 9e shows that Lake Balbina, situated in the Amazon rainforest, has experienced notable changes in LSWT over the past 21 years. The data indicates a decrease in temperature during both daytime ($p < 0.01$) and nighttime ($p < 0.05$) temperature decrease. Lake Grande do Curuai also located in the Amazon basin formed by floodplain, thus similar annual variation of LSWT to Lake Balbina was exhibited with obvious temperature decrease trend for both daytime and nighttime measurements, but not statistically significant in nighttime (Fig. 9f).

3.3.6. Typical lake from Oceania

Fig. 10a-b illustrates an increase in LSWT for nighttime measurements in both Lake Lefroy and Cowan. Interestingly, a contrasting trend is observed for Lake Cowan during daytime measurements. It can be seen from Fig. 10c-d that large LSWT variations for the daytime measurements were exhibited with Lake Eyre and Lake Corangamite, but

relative stable trends were revealed for the nighttime measurements. There is a noticeable decrease in nighttime LSWTs with Lake Eyre and Corangamite, while during the daytime there is a statistically significant increase specifically with Lake Corangamite. Lake Eyre and Corangamite are both ephemeral water bodies, large surface area variation is quite common for this type of shallow lakes formed in depression, thus the daytime LSWT shows strong fluctuation corresponding to the water surface and water volume (Song et al., 2016). The nighttime LSWT for these ephemeral lakes remains relatively stable.

4. Discussion

4.1. Regulating factors versus global LSWT pattern

This section will explore the key factors that impact the pattern, focusing on latitude, climatic regions, elevation and land use/land cover. The spatial relationship between latitudinal zones (Fig. S7a), Köppen-Geiger Climate Classification (Fig. S7b), elevation (Fig. S7c), and land use/land cover types (Fig. S7d) and the corresponding lakes were demonstrated in the supplementary material.

4.1.1. Latitudinal influences

Fig. S7a shows that lakes in the high and low latitudes have a more convergent LSWT variation, whereas water bodies in the mid latitude exhibit a larger LSWT variation. As shown in Fig. 11a, the lowest LSWT was measured with water bodies in the high latitude in the northern hemisphere ranging between $-2.62 \sim -4.79^\circ\text{C}$ with MODIS thermal sensor. The averaged daytime and nighttime LSWTs in the low latitude of northern hemisphere tend to be higher compared to those in the

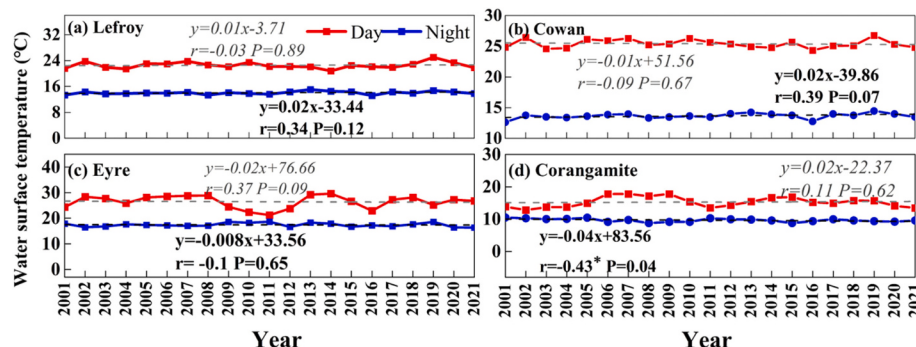


Fig. 10. Inter-annual temperature variations of lakes from Oceania.

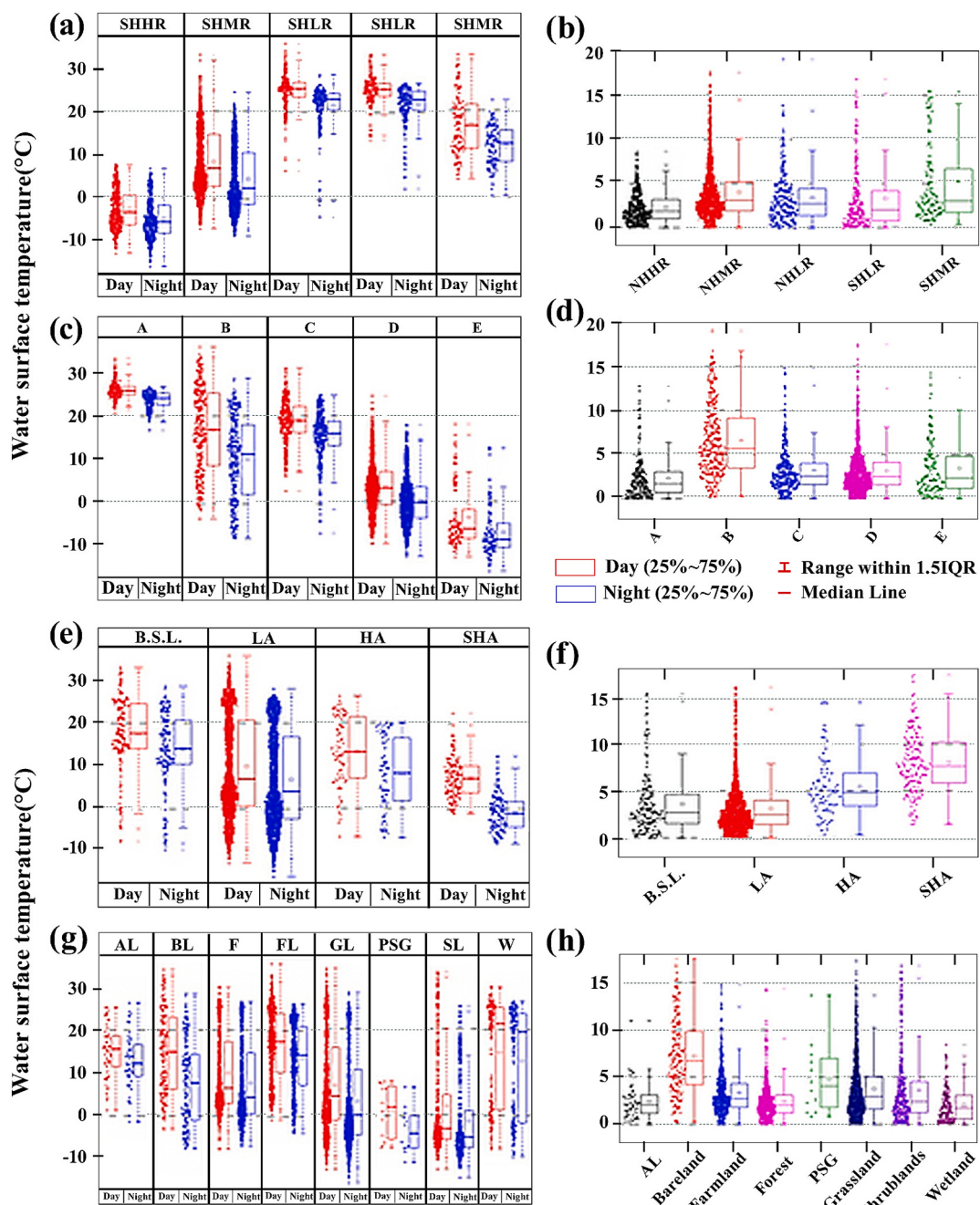


Fig. 11. Latitude Zone (a-b), Climate Zone (c-d), Altitude (e-f), Land Cover (g-h). (a-b): NHHR = Northern high latitude, NHMR = Northern middle latitude, NHLR = Northern low latitude, SHLR = Southern low latitude, SHMR = Southern middle latitude; (c-d): A = Tropical climate, B=Dry climate, C = Temperate climate, D=Boreal climate, E = Polar climate; (e-f): B.S.L. = Below sea level, LA = Low altitude, HA = High altitude, SHA = Super high altitude; (g-h): AL = Artificial land, BL = Breland, F = forest, FL = Farmland, GL = Grassland, PSG = glacier and snow, SL = Shrubland Forest, W = Wetland. - represents the maximum or minimum value, \times represents the 99 % or 1 % value, and \square represents the mean value.

southern hemisphere. While an inverse trend is observed for LSWT of water bodies in the mid latitude, the daytime LSWT of southern hemisphere (23.83°C) is higher than that in the northern hemisphere (19.05°C), likewise, nighttime shows the same trend. In total, there are 1767 lakes in the northern hemisphere of mid latitude, accounting for 70.8 % of the total. The average LSWT in these water bodies ranges from 11 to 24°C . On the other hand, there are only 169 water bodies in the southern hemisphere, with LSWT ranging from 13 to 28°C . The smallest DTDs ($0.5\text{--}2^{\circ}\text{C}$) were measured by MODIS LST for water bodies in the high latitude (Fig. 11b), followed by low latitude in the southern hemisphere ($0.5\text{--}2^{\circ}\text{C}$), and northern hemisphere ($0.5\text{--}4^{\circ}\text{C}$). The large

variations for LSWT in the mid latitude are further confirmed by larger DTDs in the northern ($1.5\text{--}4.5^{\circ}\text{C}$) and southern hemisphere ($2\text{--}8^{\circ}\text{C}$). Therefore, it can be inferred that the fluctuation in air temperature due to solar radiation across different latitudes is also responsible for the variation in LSWT with bodies of water.

4.1.2. Climatic zones

The Köppen-Geiger climatic Classification is different from latitudinal zones as they take into account both temperature and precipitation factors. This means they have stronger connection with LSWT of global water bodies (Fig. S7b). Fig. 11c-d illustrates the convergence of

LSWTs in different climate zones. In the tropical climate (A), temperate climate (C), boreal climate (D), and polar climate (E), the LSWTs show a higher level of convergence. However, in the dry climate zone (B), the variation of LSWT is more scattered. The daytime and nighttime LSWTs are 25.93 °C, 23.7 °C, respectively with the tropical climate, while lower LSWT was measured in the polar climate region, with annual average daytime and nighttime temperatures are −3.6, and −6.99 °C, respectively. Large LSWT range (2–25 °C) was encountered with lakes in the dry climate zone, while smallest LSWT range (23–27 °C) is recorded in tropical climate region, with the LSWTs of other climate zones are in between. As expected, the dry climate zone exhibited the largest DTDs when measuring lakes (2.5–7 °C). In contrast, the tropical climate zone displayed smaller DTDs (0.5–2.5 °C), while the DTDs of the remaining climate zones fell somewhere in between. This trend aligns with the findings of Schneider and Hook (2010), who highlighted that tropical lakes are particularly sensitive to climate warming due to intense solar radiation and minimal seasonal temperature fluctuations. Globally, the warming in the middle and high latitudes of the Northern Hemisphere is much higher than that in the low latitudes and the Southern Hemisphere.

4.1.3. Elevation influences

Based on the elevation threshold, Fig. S7c illustrates the division of five zones. The analysis of LSWT statistics was conducted for elevation zone. With the elevation increasing, the LSWT decreases, and the highest LSWT was measured with elevation lower than sea surface (daytime 17.41 °C; nighttime: 13.97 °C). Based on our investigation, it was found that a significant number of lakes, specifically 83 % or 2172, are located in a wide territory with elevations ranging from 0 to 1500 m. In this particular zone, we observed the largest range of LSWT (−7–20.5 °C), while the LSWT ranges in the other three elevation zones are comparatively smaller (Fig. 11e). As shown in Fig. 11f, the DTDs in minus elevation (3.45 °C) and the elevation range between 0 and 1500 m (3.05 °C) show comparative values, while highest value (8.06 °C) was measured with the higher elevation range (3500–5500 m). The influences of elevation on LSWT holds the same mechanism with climate zone, where higher air temperature results in higher LSWT, and vice versa. Noori et al. (2023) found that temperature variations in high-altitude lakes can be more pronounced between surface and deep water layers, potentially disrupting ecosystem dynamics. During warm seasons, shallower lakes are particularly susceptible to rapid temperature increases.

4.1.4. Land use/land cover influences

According to land cover data set, a total of eight major land use/land cover categories were identified (Fig. S7d). As shown in Fig. 11g, the LSWTs with glacier and snow, farmland, shrublands and artificial land show less variation. In contrast, the LSWTs with grassland, bare land, forest and wetlands show relatively larger variation. During the daytime, lakes that are surrounded by farmland, artificial land, and bare land tend to have higher land surface temperatures. The annual averages for these areas are 16.9 °C, 15.06 °C, 14.87 °C, respectively. In addition to farmland and artificial land, the LSWT surrounded by wetlands also show higher values for the nighttime MODIS measurement. It is reasonable that the lowest LSWTs were measured with lakes surrounded by glacier and snow (1.13 °C), followed by shrublands (2.09 °C) and grassland (6.93 °C) in the daytime, while minus values were measured during the nighttime for glacier and snow, and shrublands. Fig. 11h shows that lakes surrounded by bare land have larger DTDs (7.16 °C). This aligns with the findings observed in dry climates (Fig. 11d), as bare land is primarily composed of deserts. The arable land usually distributed in temperate or tropical regions, similarly residential area (major artificial land types) also has strong connection with arable land in space, thus higher LSWTs were observed for lakes surrounded by these two types of land use/land cover. In addition, the urban heat island effect can contribute to the increase in water temperature, as there is a

strong correlation between air temperature and LSWT (Song et al., 2016).

4.2. Climatic zones and air temperature

Air temperature plays a crucial role in regulating the LSWT on a global scale. While elevation and latitudinal factors do play a role in influencing LSWT, the primary reason can still be attributed to air temperature. Fig. 12 indicate a strong correlation between LSWT and air temperature across different time periods. Notably, the goodness of fit between LSWT and temperature is higher at night ($R^2 = 0.90$) compared to daytime ($R^2 = 0.80$). This difference is primarily attributed to the influence of diurnal variations in solar radiation on atmospheric conditions (Mortimer, 1987). During the day, strong solar radiation creates a more complex atmospheric environment, with temperature fluctuations influenced by meteorological factors such as cloud cover and wind speed (Reinart and Reinhold, 2008). In contrast, at night, when solar radiation weakens, the atmosphere stabilizes, resulting in more gradual temperature variations. The strong correlation between LSWT and air temperature further supports the notion that global net thermal radiation patterns play a dominant role in controlling the spatial distribution of lake temperatures (Schneider et al., 2009).

According to findings from Tibetan Plateau (Song et al., 2016), the air temperature slope caused by elevation is the major controlling factor for the alpine LSWT variation on the plateau. The lower LSWT for lakes over the Andes, the Alps, and the Pamir can also be ascribed to the high elevation. Based on the research conducted by Gorham (1964), lakes with a larger volume tend to have a higher heat budget. This suggests that Lake Qinghai would likely have a lower temperature compared to Lake Nam Co. The same principle applies to Lake Yamdrok when compared to Lake PumuYumco. However, an inverse trend was exhibited mainly due to high elevation resulting in low air temperature, which causes cooling effect on lake water temperature. The air temperature lapse rate for the mountainous area with elevation ranging from 2000 to 6000 m is about 5–6 °C/1000 m (Jacobson et al., 2005), thus the elevation differences for these two pairs of lakes may be one of the predominant reasons for the temperature differences. Rising temperatures exert a significant influence on LSWT, particularly in temperate and subtropical regions. In the context of global climate change, LSWT exhibits heightened sensitivity to air temperature fluctuations, with a 1 °C increase in air temperature resulting in a 0.78–0.92 °C rise in water temperature (Schneider et al., 2009; Woolway et al., 2020). Research indicates that as temperatures continue to rise, lake surface temperatures exhibit a more pronounced warming trend during summer, accompanied by significant alterations in thermal stratification patterns. These changes not only modify the physical structure of lakes but also have profound implications for their ecological functions and biodiversity (Sharma et al., 2019).

4.3. Lake morphology

As shown in Fig. 12, it is evident that while the LSWT closely aligns with the air water area, there are certain regions where the LSWT does not accurately reflect the air temperature. This suggests that factors other than air temperature play a role in determining the LSWT for these lakes. We collected lake morphological data from 128 bodies of lake in the Northern Hemisphere and 29 in the Southern Hemisphere. The LSWT lakes are the dependent variable in this study. The independent variables consist of lake surface area, volume, average depth, elevation of lake or reservoir surface above sea level and air temperature. The slopes for each variable (coefficients) and its corresponding significance (p -value) were listed in Table 2 below. Our analysis revealed distinct hemispheric differences in the relationships between lake characteristics and LSWT. In the Northern Hemisphere, air temperature demonstrated is positively related to LSWT ($p < 0.01$), followed by weaker but still positive associations with lake volume and elevation. Conversely,

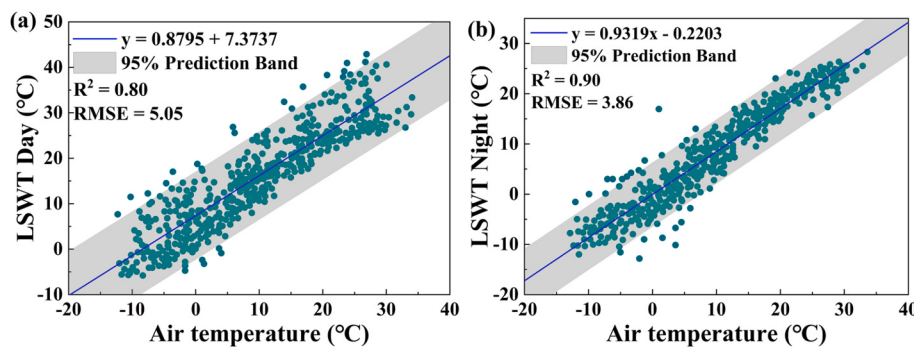


Fig. 12. The correlation between lake surface temperature and air temperature (a) daytime, (b) nighttime measurements.

Table 2

The multivariate regression models with the slope coefficients and *p*-values for each variable in both Northern Hemisphere and Southern Hemisphere.

Region	Northern Hemisphere		Southern Hemisphere	
	Index	P-value	Coefficients	P-value
Elevation	0.023575077	0.000456971	0.194164547	0.000524916
Mean depth	0.080578002	-0.004246894	0.906239023	0.000647066
Surface area	0.487905265	-1.265556E-05	0.936748879	-2.20881E-06
Volume	0.494131079	6.35933E-05	0.765281022	6.30685E-05
Air temperature	6.55448E-46	0.730255885	2.53373E-13	0.80616709

surface area and mean depth showed negative correlations with LSWT ($p > 0.05$). The Southern Hemisphere exhibited a different correlation pattern: while air temperature remained the most significant predictor ($p < 0.01$), the relationships of other variables differed substantially. Elevation, volume, and mean depth all showed positive correlations with LSWT ($p > 0.05$), while surface area maintained a negative association. This hemispheric discrepancy may be attributed to the asymmetry of land distribution and differences in climate characteristics between the Northern and Southern Hemispheres (O'Reilly et al., 2015). The relationship between volume and LSWT is positively correlated, as larger volumes have a greater capacity to store heat. According to Gorham (1964), the annual heat budgets of lakes were strongly dependent on mean depth because deeper water column maintain larger storage of heat capacity. Additional energy is required to increase the temperature of deep and large lakes. Therefore, lakes with a large volume, such as Lake Qinghai exhibited fewer temporal variations. It is important to consider other factors, such as the ratio of area to mean depth, and shoreline characteristics, that may influence this phenomenon. As the extreme case, Lake Eyre exhibited the highest temperature (Max: 25.1 °C; Mean of ice-free season, MIFS: 15.54 °C), which is also the shallowest (around 1 m) lake at lowest elevation (2678 m), which is consistent with findings from Lake Dabsun in Tibet Plateau (Song et al., 2016). Similarly, the highest temperature and DTDs were also revealed by Lake Corangamite and Asto Pan Lake, which also can be attributed to shallow water depth with small water storage.

4.4. Hydrological conditions and salinity

As depicted in Figs. 11–12, the variation in LSWT cannot be fully explained by air temperature and lake morphology factors alone. Research has shown that the source of water supply and the level of salinity in the water can also have an impact on LSWT (Ke and Song, 2014). Investigations proved that water supplying source and water salinity may also affect LSWT (Zhang et al., 2014). Despite being situated at a relatively low elevation of 3876 m; the temperature of Lake Ayakekumu is lower compared to other lakes at similar elevations and depths of 10 m. A low temperature is expected as the main water supply to the lake originates from melting glacier (Zhang et al., 2011). Located in the Pamirs, Lake Issykul remains ice-free even during the winter

season when the air temperature drops below 0 °C. High salinity is one of the reasons, while water supply source may be the other major controlling factor for the ice-free coverage in the alpine lake. Likewise, the same reason can be ascribed to Great Salt Lake for the ice free all year long. It is well-established that the salinity of water affects the temperature at which ice forms. Therefore, lakes with high salinity can anticipate a longer duration without ice (Wang and Dou, 1998). The relatively longer ice-free season for Lake Van, Lake Utah, Lake Pyramid is also can be ascribed to the high salinity in these lakes. The speculation for some of the lakes needs to be further investigated for the saline effect on water temperature.

The MODIS WST monitoring method proposed in this study offers direct practical applicability. It is based on publicly available MODIS LST products, ensuring global generalizability. Furthermore, we provide a complete and reproducible workflow (see Supplementary Materials Fig. S1), making it readily implementable. This approach is suitable for various management needs, including fisheries assessment and algal bloom early warning. However, the current 1 km spatial resolution poses limitations for monitoring small lakes. In the future, integrating multi-source data such as Sentinel-3 could enhance monitoring accuracy, thereby better supporting operational demands in national water resource management.

5. Conclusions

In summary, this study is to evaluate the global LSWT of lakes larger than 25 km² using 12,978 tiles of the MODIS LST product. The global spatial LSWT pattern for lakes larger than a certain threshold indicates that the distribution of solar radiation is the key regulating factor controlling LSWT. A strong relationship between air temperature and LSWT was revealed, with nighttime measurements showing a higher correlation ($R^2 = 0.90$) than daytime measurements ($R^2 = 0.80$). The study also found that various lake characteristics, such as orientation and water sources, contribute to the temporal and spatial variation in LSWT. However, these factors account for only a small portion of the overall variation on a global scale. Additionally, factors such as water salinity and groundwater supply may influence LSWT. The inter-annual variations of the LSWT for typical lakes from different continents were derived from time series data set of 8-day composite MODIS LST

products during 2001–2021. Out of the 46 lakes studied, the results showed that 9 of them experienced a decrease in LSWT over the past 21 years. These lakes are primarily located in the Great Rift Valley region. On the other hand, 13 of the lakes showed a clear increase in LSWT, with most of them being situated in high latitude areas. The remaining 24 lakes did not exhibit a noticeable trend in LSWT, suggesting a relatively stable pattern over the past 21 years. In addition, this investigation revealed that lakes in tropical and polar climates displayed significantly smaller DTDs, whereas water bodies in arid climates exhibited the opposite pattern. It is worth mentioning that deep and large lakes with a significant volume have small DTDs, whereas shallow water bodies have larger DTDs due to their lower heat capacity. This study demonstrates that remote sensing using MODIS LST products effectively captures the spatial and temporal variability of LSWT on a continental scale, contributing to a deeper understanding of the processes controlling large-scale LSWT variability.

CRediT authorship contribution statement

Boyu Zhao: Writing – original draft, Software, Investigation. **Zhongqiu Sun:** Writing – review & editing, Supervision. **Min Wang:** Software, Formal analysis. **Jia Du:** Writing – review & editing. **Kaishan Song:** Writing – review & editing, Supervision, Funding acquisition.

Declaration of competing interest

The authors declare that they have no known competing financial interests or personal relationships that could have appeared to influence the work reported in this paper.

Acknowledgements

This research was financially supported by the Natural Science Foundation of China (U2243230, 42171374), Jilin Provincial Department of Ecology and Environment (2024-01), Young Scientist Group Project of Northeast Institute of Geography and Agroecology, Chinese Academy of Sciences (2023QNXZ01), and Jilin Provincial Key Laboratory of Remotely Sensed Big Data for Ecology and Environment Research.

Appendix A. Supplementary data

Supplementary data to this article can be found online at <https://doi.org/10.1016/j.ecoinf.2025.103184>.

Data availability

All MODIS images were obtained from the GEE at <https://earthengine.google.com/>, Latitude data was obtained from NASA's Earth Observing System Data and Information System, at <https://earthdata.nasa.gov/>. Climate zone data was sourced from the Köppen-Geiger Climate Classification at <https://www.climatemp.com/>. Elevation data was derived from the Advanced Spaceborne Thermal Emission and Reflection Radiometer Global Digital Elevation Model (ASTER GDEM) with a 30-m resolution, at <https://asterweb.jpl.nasa.gov/gdem.asp>. The land-cover data were obtained from the Aerospace Information Research Institute, CAS, at <https://zenodo.org/records/8239305>. The developed GLAST dataset can be accessed through <https://zenodo.org/record/8322038>.

References

- Adrian, R., O'Reilly, C.M., Zagarese, H., Baines, S.B., Hessen, D.O., Keller, W., Winder, M., 2009. Lakes as sentinels of climate change. *Limnol. Oceanogr.* 54 (6part2), 2283–2297.
- Bussières, N., Versegheghy, D., MacPherson, J.I., 2002. The evolution of AVHRR-derived water temperatures over boreal lakes. *Remote Sens. Environ.* 80 (3), 373–384.
- Gibbons, J.K., Bridgeman, B.T., 2020. Effect of temperature on phosphorus flux from anoxic western Lake Erie sediments. *Water Res.* 182, 116022.
- Gizińska, J., Sojka, M., 2023. How climate change affects river and lake water temperature in central-West Poland—a case study of the Warta River catchment. *Atmosphere* 14 (2), 330.
- Gorham, E., 1964. Morphometric control of annual heat budgets in temperate lakes. *Limnol. Oceanogr.* 9 (4), 529–533.
- Hampton, S., Izmesteva, L.R., Moore, M.V., Katz, S.L., Dennis, B., Silow, E.A., 2008. Sixty years of environmental change in the world's largest freshwater Lake – Lake Baikal, Siberia. *Glob. Chang. Biol.* 14, 1947–1958.
- Huang, L., Wang, X., Yan, Y., Jin, L., Yang, K., Chen, A., Piao, S., 2023. Attribution of lake surface water temperature change in large lakes across China over past four decades. *J. Geophys. Res. Atmos.* 128 (21), e2022JD038465.
- Hulley, G.C., Hook, S.J., Schneider, P., 2011. Optimized split-window coefficients for deriving surface temperatures from inland water bodies. *Remote Sens. Environ.* 115, 3758–3769.
- Ibrahim, Majed, et al., 2020. An evaluation of available digital elevation models (DEMs) for geomorphological feature analysis. *Environ. Earth Sci.* 79 (13), 336.
- Jacobson, L.D., Hetchler, B.P., Johnson, V.J., 2005. Spatial, diurnal, and seasonal variations of temperature, ammonia, and hydrogen sulfide concentrations in two tunnel ventilated sow gestation buildings in Minnesota. In: Livestock Environment VII, 18-20 May 2005, Beijing, China. American Society of Agricultural and Biological Engineers, p. 198.
- Jeppesen, E., Meerhoff, M., Davidson, T., Trolle, D., Sondergaard, M., Lauridsen, T., Nielsen, A., 2014. Climate change impacts on lakes: an integrated ecological perspective based on a multi-faceted approach, with special focus on shallow lakes. *J. Limnol.* 73.
- Jungkeit-Milla, K., Pérez-Cabello, F., de Vera-García, A.V., Galofré, M., Valero-Garcés, B., 2024. Lake surface water temperature in high altitude lakes in the Pyrenees: combining satellite with monitoring data to assess recent trends. *Sci. Total Environ.* 933, 173181.
- Justice, C.O., Vermote, E., Townshend, J.R.G., et al., 1998. The moderate resolution imaging Spectroradiometer (MODIS): land remote sensing for global change research. *IEEE Trans. Geosci. Remote Sens.* 36 (4), 1228–1249.
- Ke, L.H., Song, C.Q., 2014. Remotely sensed surface temperature variation of an inland saline lake over the central Qinghai-Tibet Plateau. *ISPRS J. Photogramm. Remote Sens.* 98, 157–167.
- Korver, M.C., Lehner, B., Cardille, J.A., Carrea, L., 2024. Surface water temperature observations and ice phenology estimations for 1.4 million lakes globally. *Remote Sens. Environ.* 308, 114164.
- Kraemer, B.M., Pilla, R.M., Woolway, R.I., Anneville, O., Ban, S., Colom-Montero, W., Adrian, R., 2021. Climate change drives widespread shifts in lake thermal habitat. *Nat. Clim. Chang.* 11 (6), 521–529.
- Lehner, B., Döll, P., 2004. Development and validation of a global database of lakes, reservoirs and wetlands. *J. Hydrol.* 296 (1–4), 1–22.
- Livingstone, D.M., 2003. Impact of secular climate change on the thermal structure of a large temperate central European lake. *Clim. Chang.* 57 (1–2), 205–225.
- Mortimer, C.H., 1987. Fifty years of physical investigations and related limnological studies on Lake Erie, 1928–1977. *J. Great Lakes Res.* 13 (4), 407–435.
- Noori, R., Woolway, R.I., Jun, C., Bateni, S.M., Naderian, D., Partani, S., Pulkkanen, M., 2023. Multi-decadal change in summer mean water temperature in Lake Konnevesi, Finland (1984–2021). *Eco. Inform.* 78, 102331.
- O'Reilly, C.M., Sharma, S., Gray, D.K., Hampton, S.E., Read, J.S., Rowley, R.J., Zhang, G., 2015. Rapid and highly variable warming of lake surface waters around the globe. *Geophys. Res. Lett.* 42 (24), 10–773.
- Peel, M.C., Finlayson, B.L., McMahon, T.A., 1998. Updated world map of the Köppen-Geiger climate classification. *Hydrocl. Earth Syst. Sci.* 11 (5), 1633–1644.
- Pekel, J.F., Cottam, A., Gorelick, N., Belward, A.S., 2016. High-resolution map of global surface water and its long-term changes. *Nature* 540 (7633), 418–422.
- Peng, Z., Yang, K., Shang, C., Duan, H., Tang, L., Zhang, Y., Luo, Y., 2022. Attribution analysis of lake surface water temperature changing—taking China's six main lakes as example. *Ecol. Indic.* 145, 109651.
- Piccolroaz, S., Zhu, S., Ludwig, R., Carrea, L., Oliver, S., Piotrowski, A.P., Zhu, D.Z., 2024. Lake water temperature modeling in an era of climate change: data sources, models, and future prospects. *Rev. Geophys.* 62 (1), e2023RG000816.
- Ptak, M., Olowoyele, T., Sojka, M., 2022. Trends of changes in minimum lake water temperature in Poland. *Appl. Sci.* 12 (24), 12601.
- Reinart, A., Reinhold, M., 2008. Mapping surface temperature in large lakes with MODIS data. *Remote Sens. Environ.* 112 (2), 603–611.
- Schneider, P., Hook, S.J., 2010. Space observations of inland water bodies show rapid surface warming since 1985. *Geophys. Res. Lett.* 37 (22).
- Schneider, P., Hook, S.J., Radocinski, R.G., Corlett, G.K., Hulley, G.C., Schladow, S.G., Steissberg, T.E., 2009. Satellite observations indicate rapid warming trend for lakes in California and Nevada. *Geophys. Res. Lett.* 36 (22).
- Sharma, S., Blagrave, K., Magnuson, J.J., O'Reilly, C.M., Oliver, S., Batt, R.D., Woolway, R.I., 2019. Widespread loss of lake ice around the northern hemisphere in a warming world. *Nat. Clim. Chang.* 9 (3), 227–231.
- Song, K.S., Wang, M., Du, J., Yuan, Y., Ma, J., Wang, M., Mu, G., 2016. Spatiotemporal variations of lake surface temperature across the Tibetan plateau using MODIS LST product. *Remote Sens.* 8 (10), 854.
- Tong, Y., Feng, L., Wang, X., Pi, X., Xu, W., Woolway, R.I., 2023. Global lakes are warming slower than surface air temperature due to accelerated evaporation. *Nat. Water* 1 (11), 929–940.
- Trumpickas, J., Shuter, B.J., Minns, C.K., Cyr, H., 2015. Characterizing patterns of nearshore water temperature variation in the north American Great Lakes and assessing sensitivities to climate change. *J. Great Lakes Res.* 41, 53–64.

- Verburg, P., Hecky, R.E., Kling, H., 2003. Ecological consequences of a century of warming in Lake Tanganyika. *Science* 301 (5632), 505–507.
- Wan, Z., Zhang, Y., Zhang, Q., Li, Z.L., 2002. Validation of the land surface temperature products retrieved from terra moderate resolution imaging spectroradiometer data. *Remote Sens. Environ.* 83, 163–180.
- Wang, S.M., Dou, H.S., 1998. Chinese Lakes Inventory. Science Press, Beijing, China.
- Wang, R., Dong, W., Sun, J., Sojka, M., Ptak, M., Zhu, S., 2025. Long-term trends of lake surface water temperatures in lowland polish temperate lakes. *Atmosphere* 16 (2), 120.
- Woolway, R.I., Merchant, C.J., 2019. Worldwide alteration of lake mixing regimes in response to climate change. *Nat. Geosci.* 12 (4), 271–276.
- Woolway, R.I., Kraemer, B.M., Lengers, J.D., Merchant, C.J., O'Reilly, C.M., Sharma, S., 2020. Global lake responses to climate change. *Nat. Rev. Earth Environ.* 1 (8), 388–403.
- Yang, K., Qin, J., Hou, J., Lei, Y., Wang, J., Huang, A., Li, X., 2022. A strict validation of MODIS lake surface water temperature on the Tibetan Plateau. *Remote Sens.* 14 (21), 5454.
- Yin, H., Yin, P., Yang, Z., 2023. Seasonal sediment phosphorus release across sediment-water interface and its potential role in supporting algal blooms in a large shallow eutrophic Lake (Lake Taihu, China). *Sci. Total Environ.* 896, 165252.
- Zhang, G., Xie, H., Kang, S., Yi, D., Ackley, S.F., 2011. Monitoring lake level changes on the Tibetan Plateau using ICESat altimetry data (2003–2009). *Remote Sens. Environ.* 115, 1733–1742.
- Zhang, G., Yao, T., Xie, H., Qin, J., Ye, Q., Dai, Y., Guo, R., 2014. Estimating surface temperature changes of lakes in the Tibetan Plateau using MODIS LST data. *J. Geophys. Res. Atmos.* 119, 8552–8567.
- Zhou, B., Xu, Y., Wu, J., Dong, S., Shi, Y., 2015. Changes in temperature and precipitation extreme indices over China: analysis of a high-resolution grid dataset. *Int. J. Climatol.* 36 (3).
- Zhu, S., Ptak, M., Sojka, M., Piotrowski, A.P., Luo, W., 2023. A simple approach to estimate lake surface water temperatures in polish lowland lakes. *J. Hydrol. Region. Stud.* 48, 101468.